Nuclear Inst. and Methods in Physics Research, A 898 (2018) 53–59

Contents lists available at ScienceDirect

Nuclear Inst. and Methods in Physics Research, A

journal homepage: www.elsevier.com/locate/nima

Radiation hardness of gallium doped low gain avalanche detectors☆

G. Kramberger [a,*], M. Carulla [b], E. Cavallaro [c], V. Cindro [a], D. Flores [b], Z. Galloway [e], S. Grinstein [c,d], S. Hidalgo [b], V. Fadeyev [e], J. Lange [c], I. Mandić [a], A. Merlos [b], F. McKinney-Martinez [e], M. Mikuž [a,f], D. Quirion [b], G. Pellegrini [b], M. Petek [a], H.F.-W. Sadrozinski [e], A. Seiden [e], M. Zavrtanik [a]

[a] Jožef Stefan Institute, Jamova 39, SI-1000 Ljubljana, Slovenia
[b] Centro Nacional de Microelectrónica (IMB-CNM-CSIC), Barcelona 08193, Spain
[c] Institut de Física d'Altes Energies (IFAE), The Barcelona Institute of Science and Technology (BIST), 08193 Bellaterra (Barcelona), Spain
[d] Institució Catalana de Recerca i Estudis Avançats (ICREA), Pg. Lluís Companys 23, 08010 Barcelona, Spain
[e] UCSC, Santa Cruz Institute for Particle Physics, Santa Cruz, CA 95064, USA
[f] University of Ljubljana, Faculty of Mathematics and Physics, Jadranska 19, SI-1000 Ljubljana, Slovenia

ARTICLE INFO

Keywords:
Silicon detectors
Radiation damage
Charge multiplication
Acceptor removal

ABSTRACT

Low Gain Avalanche Detectors (LGADs) are based on a n^{++}-p^{+}-p-p^{++} structure where appropriate doping of multiplication layer (p^{+}) leads to high enough electric fields for impact ionization. Operation of these detectors in harsh radiation environments leads to decrease of gain attributed to the effective acceptor removal in the multiplication layer. In order to cope with that devices were produced where boron was replaced by gallium. The initial radiation hardness studies show a smaller degradation of gain with neutron fluence indicating that gallium is more difficult to displace/deactivate from the lattice site than boron.

1. Introduction

Low gain avalanche detectors (LGAD) exploit n^{++}-p^{+}-p-p^{++} structure to achieve high enough electric field near the junction contact for impact ionization [1]. The gain depends on the p^{+} layer's doping level, profile shape, device thickness and applied bias voltage. Usually gain factors of several tens were achieved in most LGADs produced so far [1–3]. This enables efficient operation of thin sensors required for precise timing applications in particle physics [4,5]. A superb timing resolution of 26 ps per single LGAD layer has been achieved recently [6,7], which made thin LGADs the baseline option for timing detectors in end-caps of both CMS [8] and ATLAS [9] after luminosity upgrade of LHC (HL-LHC) in 2024. The main obstacle for their successful use in future high energy physics experiments is their degradation of gain with fluence. At HL-LHC LGADs will be exposed to equivalent fluences of up to $\Phi_{eq} = 6 \cdot 10^{15}$ cm^{-2}. At these fluences, the gain from the p^{+} layer completely disappears [2,10]. Irradiation induced deep acceptors in the bulk compensate partially the loss of gain layer [2,7] at high fluences ($\Phi_{eq} > 2 \cdot 10^{15}$ cm^{-2}), but for substantial gain operation very close to the breakdown voltage is nevertheless required. Therefore, a way to mitigate the gain loss with radiation is sought.

The gain loss is attributed to the removal of effective acceptors in the multiplication layer which leads to a reduction of the peak electric fields. Although there were different approaches proposed to mitigate the acceptor removal, a replacement of boron with gallium appears to be a logical choice. It was observed before that initial acceptor removal is smaller for gallium than for boron doped silicon after electron irradiation in solar cells [11], but measurements with detector grade gallium doped diodes are very scarce. Gallium is heavier than boron and thus more difficult to displace from the lattice site and could be less susceptible to reactions with vacancies in the Si lattice (V) and interstitial silicon atoms (I).

In this paper we show first results of irradiated LGADs produced with gallium replacing boron as dopant in the multiplication layer.

2. Samples and experimental technique

Pad detectors were produced on high resistivity p-type silicon wafers (10 kΩcm, boron doped) by CNM. The samples studied were 285 μm thick and had an active area of 3.2×3.2 mm^2. The front side of the detector had a circular opening in the center to allow for light injection,

☆ Work performed in the framework of the CERN-RD50 collaboration.
* Corresponding author.
E-mail address: Gregor.Kramberger@ijs.si (G. Kramberger).

https://doi.org/10.1016/j.nima.2018.04.060
Received 24 November 2017; Received in revised form 5 March 2018; Accepted 29 April 2018
Available online 5 May 2018

while the back side of the devices was fully metallized. Gallium was implanted by Ion Beam Services S.A., Peynier, France, at an energy of 195 keV. Four different implantation doses were used (Dose1, Dose2, Dose3 and Dose4), with a difference of around 25% between the highest (Dose4) and lowest dose (Dose1). The subsequent diffusion and activation process of gallium was the same for all implantation doses resulting in foreseen $\sim$ 4 μm deep implant with peak concentration of order $10^{16} - 10^{17}$ cm^{-3}. Apart from devices with multiplication layer also control/no-gain devices of the same layout, but without the multiplication layer were produced for comparison.

The samples were irradiated with neutrons at the Jožef Stefan Institute research reactor [12] to equivalent fluences up to $\Phi_{eq} = 6 \cdot 10^{15}$ cm^{-2}. They were characterized by the Transient Current Technique (TCT) [13] and Charge Collection Measurement (CCM) with electrons from ^{90}Sr source using LHC speed electronics. The detailed description of the setups can be found in [14] for TCT and [15] for CCM. In the latter the source is collimated to the extent that almost all the electrons (> 97%) that reach the scintillator below the sample and trigger the readout have crossed the detector, thus allowing measurements of the signal even at small signal-to-noise ratio. The measurements were performed before any intentional annealing and after an annealing of 80 min at 60 °C.

3. Performance before irradiation

The process parameters for gallium implantation, unlike for boron, are less studied and known. As a result, the implantation profile of gallium differed from the planned one. It led to very high gain and consequently break down of the devices starting at around 30 V with a steep rise of the leakage current. This is shown in Fig. 1a.

Observations of the currents induced after illumination of junction side with pulses of red light (350 ps wide, energy ~5 pJ, $\lambda = 660$ nm, 500 Hz) confirm that the break down of the devices is due to the high gain in the multiplication region. The induced currents start to rise at the same voltages as the leakage currents. The induced charges (Q, induced current integral in 10 ns) for different detectors are shown in Fig. 1b.

The shape of the induced currents (Fig. 1c) reveals that the device behaves differently to standard LGAD detectors [10]. After sufficient depletion of the multiplication layer ($\sim 25 - 30$ V) produces a sizable gain, any further bias voltage depletes the rest of the gain layer, but the depletion region does not reach the bulk. The long tail in the induced current is the consequence of diffusion of multiplied holes over the entire thickness of the detector. For short integration times required by the operation at the LHC (< 25 ns) the charge induced at later times is lost for the measurement.

4. Charge collection and gain of LGAD devices

A reduction in gain with irradiation due to the removal of effective acceptors from the multiplication layer rendered the devices operational. The measured most probable charge of ^{90}Sr electrons in gallium doped LGADs (Ga-LGAD) is shown in Fig. 2a. For comparison, the most probable charge in boron doped devices (B-LGAD) from one of the previous runs (Run 6474, see [10]) with the same gain as targeted in the implantation process for Ga-LGAD is shown. It is clear that Ga-LGADs perform better in terms of charge collection when compared not only control/no-gain devices (see Fig. 2b), but also better than similar B-LGADs. Although, for a firm conclusion a fully operational Ga-LGAD before irradiation would be needed. After irradiation to $\Phi_{eq} = 5 \cdot 10^{14}$ cm^{-2} the most probable charge of 180 ke was collected, around three times more than for B-LGAD at 500 V. The difference is reduced to 2–3 times for $1 \cdot 10^{15}$ cm^{-2} and around twice at $2 \cdot 10^{15}$ cm^{-2}.

It is expected that this difference in gain would be magnified for thinner detectors [2,5]. The same voltage drop over a smaller thickness increases the electric field also in the multiplication layer. Subsequently, this leads to higher gain for thinner devices with the same level of doping in the gain layer [2,7].

The gain after irradiation depends on the gallium dose, as shown in Fig. 3. It can be observed that at intermediate fluences the gain for the medium gallium dose device (Dose2) is higher than for the highest gallium dose device (Dose4). The latter becomes more efficient at fluence of $2 \cdot 10^{15}$ cm^{-2}. Both devices, however, perform similar to the control device in terms of collected charge (see Fig. 2b), albeit at lower voltages, at the lowest fluence of $1 \cdot 10^{14}$ cm^{-2}. The Dose4 device exhibits similar performance also at $5 \cdot 10^{14}$ cm^{-2}, where almost entire bulk is active already at 200 V. The difference between generated (≈ 21000 e) and measured charge (≈ 15000 e) is attributed to trapping.

The reason for such behavior was investigated by TCT measurements. Red laser pulses were used for the front illumination while α particles (5.8 MeV,^{241}Am, 2 mm air gap between sensors and source) were used for the back side illumination. The penetration depth of α-s is around 20 μm. The induced currents for electron injection (α-s at the back) in the Dose2 device irradiated to $1 \cdot 10^{14}$ cm^{-2}, are shown in Fig. 4a. The current shapes are typical for carriers injected in high field region that drift towards the low field region (steady decrease of the induced current), which means that the silicon bulk has positive space charge. This is evident for the two lowest voltages shown and also for higher voltages in first few ns (< 5 ns). Moreover, the current shapes show that detector bulk is fully depleted already at relatively low voltages. This can be concluded from the steep decrease of induced current at $\sim$ 5 ns which is related to the end of electrons' drift.

At high bias voltages a second peak in the induced current emerges as a result of multiplication. The appearance of the peak is however delayed in time (> 10 ns). The current due to the multiplied holes drift shows a long tail typical for diffusion. The conclusion can be confirmed by looking at the front contact illumination (hole injection) by laser pulses in Fig. 4b. A very short induced current pulse indicates large gain, but the subsequent drift of holes is not visible. Although at 100 V the larger part of the silicon bulk is already depleted. This means that multiplied holes have to cross certain part of detector where there is no field as explained below.

Such signals can be qualitatively described by electric field shape shown in Fig. 5. The shape of the electric field in the bulk (red) roughly corresponds to the one in forward biased silicon detectors (so called Current Injected Devices, CID, studied by RD39 collaboration [16,17]), where injection of holes by forward bias is replaced by a gain layer. As soon as the multiplication layer depletes (green), high gain assures large concentration of holes near the contact. As a result in a certain part of the detector, LF (Low Field), there is very low electric field (black).

In the part of the detector with sizable electric field ($x > LF$), the trapped holes cause positive space charge. The field in the bulk should have a square root dependence on position regardless of fluence as long as it is in CID mode [16]. As the gain decreases with irradiation LF becomes narrower and when $LF = 0$ the mode of operation becomes the one of the standard LGAD. This can be seen in current pulses for α particles in the Ga-LGADs irradiated to $5 \cdot 10^{14}$ cm^{-2} (see Fig. 6). The lower initial gain for Dose1 device leads to $LF = 0$ and the sharp rise of the induced current after the electron drift is over at $t \approx 3.5$–5 ns, upon their simultaneous arrival to the multiplication region.

A slightly delayed peak for Dose2 device indicates that the low field region ($LF \rightarrow 0$) is overcome by diffusion. Further increase of implantation dose results in even larger LF for Dose3 and Dose4 devices. For the latter, the peak is small and appears only at very high bias voltages. The reason for relatively small peak in induced current for Dose4 devices, which however appears at times similar to that of the Dose3 devices, is not clear.

Unlike for laser pulses, α particles allow absolute comparison of induced currents shown in Fig. 7. It appears that electric field is almost identical (similar positive space charge) in the detector bulk for the devices with $LF \neq 0$ (Dose2,Dose3,Dose4). Only for Dose1 device at 300 V the electrons multiply immediately after the drift ends ($t \approx 5$ ns). At high bias voltages $LF = 0$ holds also for Dose2 device (gain of around 10). This can be concluded from Fig. 6b, but also from Fig. 7b, which

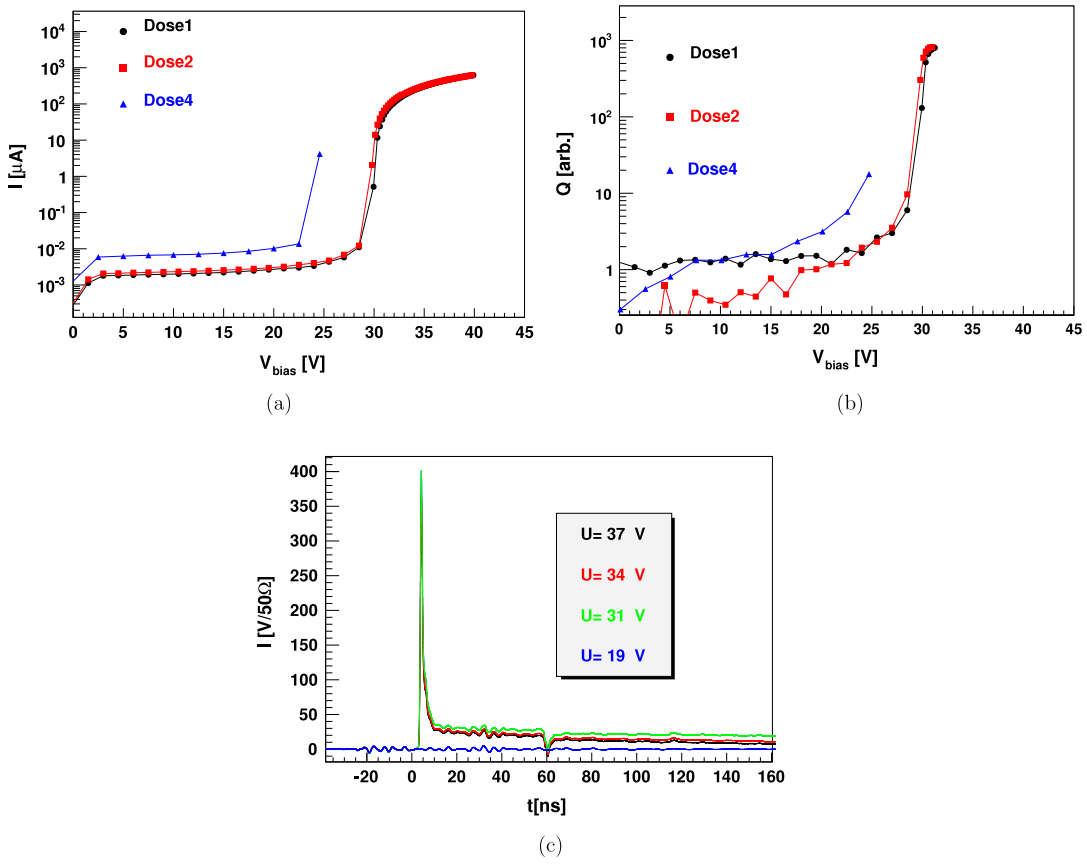

Fig. 1. (a) Dependence of leakage current on bias voltage for different gallium doped LGAD devices. (b) Collected charge (TCT) in 10 ns after illumination of the junction side of the devices shown in (a). (c) Induced current pulses for Dose1 device at different voltages. All the measurements shown were done at $T = -10$ °C.

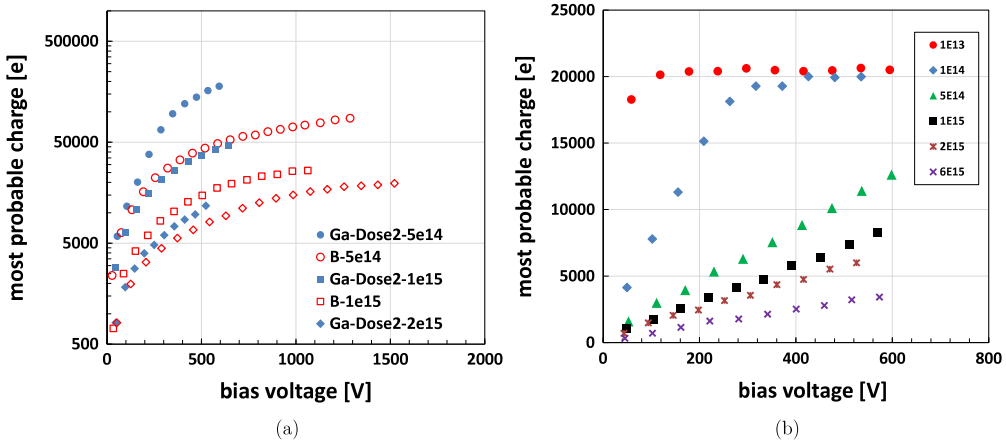

Fig. 2. (a) Most probable charge for ^{90}Sr electrons in Ga-LGADs (Dose2) irradiated to different fluences and comparison with similar B-LGADs. (b) The charge collection of control/no-gain samples at the investigated fluences in [cm^{-2}]. The measurements were taken at $T = -15$ °C. Note the logarithmic scale for the LGAD data.

shows a more efficient charge collection at high voltages of Dose2 than of Dose1 device.

At fluences of $\Phi_{eq} \geq 10^{15}$ cm^{-2} the second peak in the induced current and subsequent few ns long drift of holes, shown in Fig. 8 for Dose2 and Dose4 devices, indicate that the gain is still substantial. The gain can be estimated as the ratio of the total induced charge ($\int_0^{20\text{ ns}} I(t)dt$) and the charge coming from the drift of the injected electrons ($\int_0^{3.5\text{ ns}} I(t)dt$, i.e. before the appearance of the second peak). Values of $G \approx 1.5$ for Dose4 ($2 \cdot 10^{15}$ cm^{-2}) and $G \approx 3$ for Dose2 (10^{15} cm^{-2}) devices at 600 V set a lower limit for any carrier generation in the sensor. A more favorable generation of carriers along the ^{90}Sr electron track, where less electrons are trapped before undergoing multiplication, gives slightly higher gain values, $G \approx 2.3$ for Dose4 ($2{\cdot}10^{15}$ cm^{-2}) and $G \approx 3.3$ for Dose2 devices (10^{15} cm^{-2}). The gain values

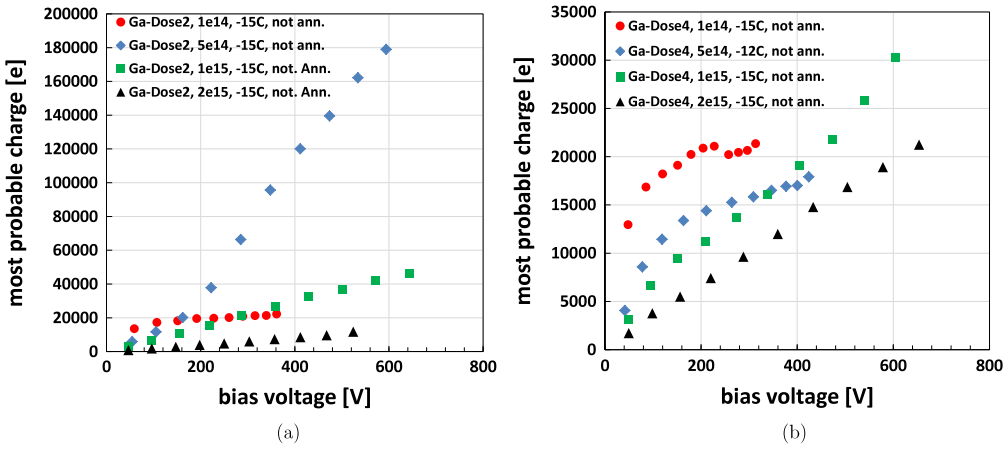

Fig. 3. (a) Dependence of most probable charge for ^{90}Sr electrons for (a) Dose2 devices and (b) Dose4 devices at different fluences in [cm^{-2}]. The devices were not intentionally annealed and were measured at $T = -15$ °C.

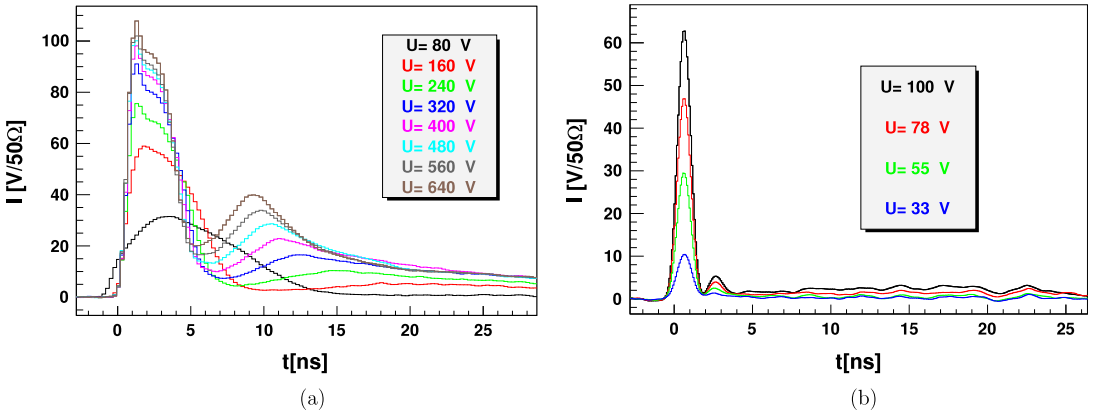

Fig. 4. (a) Induced currents in the Dose2 detector irradiated to $1 \cdot 10^{14}$ cm^{-2} exposed to ^{241}Am α particles from the backside. (b) Induced currents after illumination of the front side with light pulses. Measurements were done at $T = -10$ °C. (For interpretation of the references to colour in this figure legend, the reader is referred to the web version of this article.)

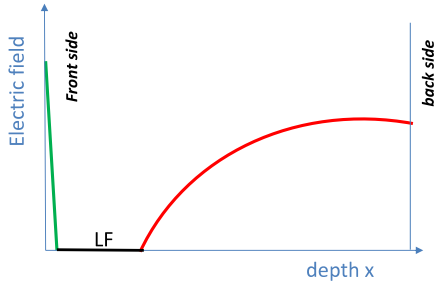

Fig. 5. Schematic shape of electric field model that corresponds to the observed signals. (For interpretation of the references to colour in this figure legend, the reader is referred to the web version of this article.)

were obtained as ratio of most probable charge measurements at 600 V in Ga-LGADs and control samples shown in Figs. 2 and 3. It should be noted, however, that the electric field profiles changed when compared to those in the devices irradiated to lower fluences (see Fig. 8).

5. Gallium removal

Significantly better performance in charge collection of irradiated Ga-LGADs than of B-LGADs can be attributed to smaller acceptor (gallium) removal as well as to much larger initial gain. Removal of gallium from the multiplication layer can be determined for devices in standard mode of operation ($LF = 0$) by using the red laser TCT. After the depletion of the multiplication layer, the depleted area extends into the bulk with further bias voltage (V_{bias}) increase. Only after this occurs, the induced charge due to the multiplied holes starts to increase (see [10]). This is a consequence of their drift over a sizable portion of the detector depth (i.e. weighting potential). Therefore, the values of voltage required for the depletion of the multiplication layer V_{mr} were obtained by fitting $Q \propto \sqrt{V_{bias} - V_{mr}}$ to the measured charge. A constant effective doping concentration in the bulk is whereby assumed. It can be seen in Fig. 9a that V_{mr} (kink in the fitted function) decreases with equivalent fluence for Dose2 devices. For comparison the measurements at $5 \cdot 10^{14}$ cm^{-2}, where $LF \neq 0$ and V_{mr} cannot be determined, is also shown.

If it is assumed that the removal of active gallium occurs with the same rate everywhere in the p$^+$ layer, then the V_{mr} is proportional to an average concentration of gallium N_{Ga} and the evolution of V_{mr} with fluence can be described as

$$N_{Ga} = N_{Ga,0}\ \exp(-c\ \Phi_{eq}) \quad \Rightarrow \quad V_{mr} \approx V_{mr,0}\ \exp(-c\ \Phi_{eq}) \quad , \tag{1}$$

where c is the removal constant, $N_{Ga,0}$ initial doping concentration and $V_{mr,0}$ the corresponding multiplication layer depletion voltage. The data and the Eq. (1) fit to the data for all four implantation doses after annealing for 80 min at 60 °C are shown in Fig. 9b (see paragraph on annealing below). The free parameters of the fit were c and $V_{mr,0}$. The obtained values of $c = 5.8, 5.6, 5.5$ and $5.1 \cdot 10^{-16}$ cm^2 for Dose1,2,3,4 devices,

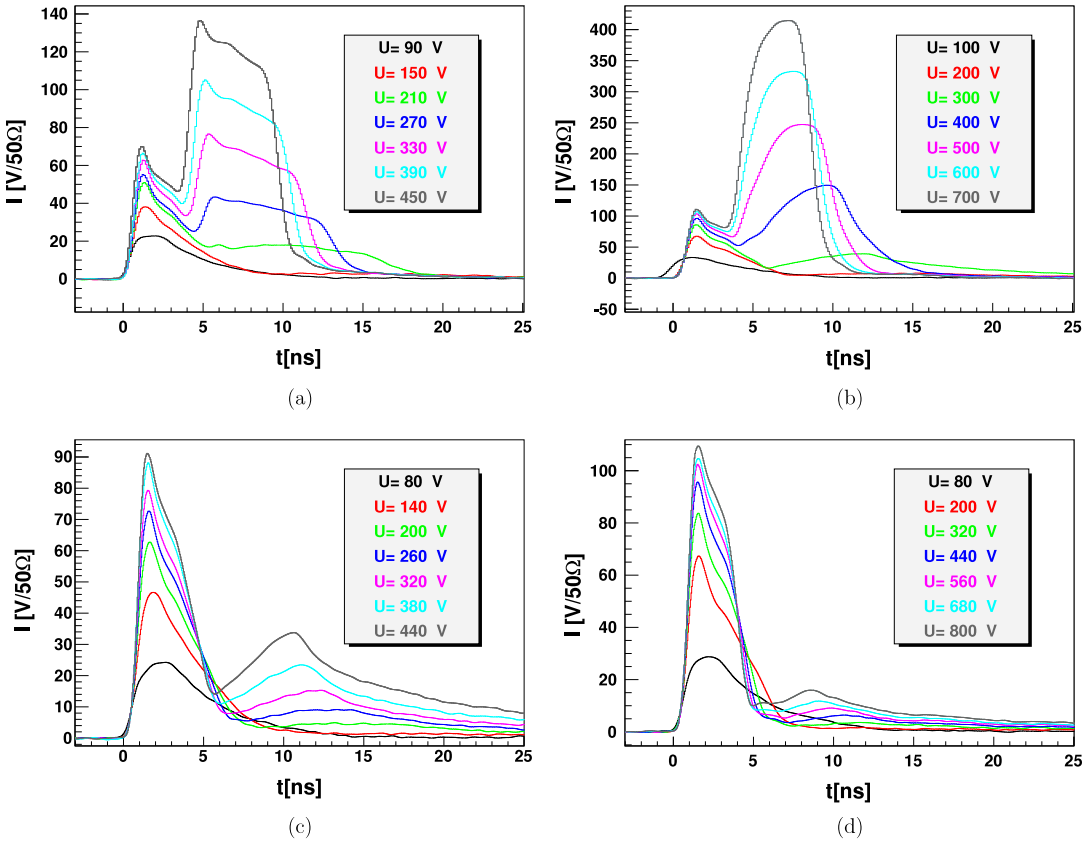

Fig. 6. Induced currents at different bias voltages after exposure of the back of the detector to α particles for: (a) Dose1, (b) Dose2, (c) Dose3 and (d) Dose4 devices irradiated to $5 \cdot 10^{14}$ cm^{-2}. Measurements were done at $T = -10$ °C.

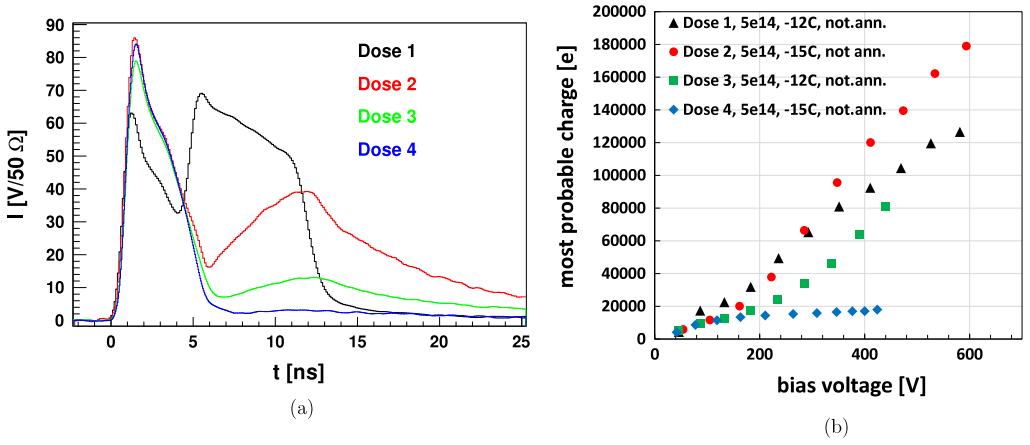

Fig. 7. (a) Comparison of induced currents for different devices irradiated to $5 \cdot 10^{14}$ cm^{-2} at 300 V and $T = -10$ °C after exposure to α particles. (b) Dependence of most probable charge of ^{90}Sr electrons on voltage for these devices.

which are around 1.5–2 times smaller than obtained for boron doped devices [10]. The extracted $V_{mr,0} = 41.5, 44.2, 47, 67$ V for Dose1,2,3,4 devices follow roughly the relative difference in initial doping with the exception of the Dose4 device, where however the uncertainty is very large due to only two points included in the fit.

The obtained values of removal rate imply that performance of the Ga-LGADs would deteriorate slower than that of the B-LGADs. The fluence range in which they outperform standard/no-gain devices would be therefore extended by almost a factor of two with respect to the B-LGADs of similar initial performance. It was shown, however, that c decreases with initial boron concentration. If the same holds also for gallium, then smaller c for gallium devices may also be (partially) attributed to larger initial concentration. This has yet to be established.

6. Short term annealing

The measurements shown so far (except Fig. 9) were done before any intentional annealing. In order to see the possible effect of short term annealing on Ga-LGAD the devices were annealed for 80 min at 60 °C, which is enough to complete the short term annealing in B-LGAD devices. Contrary to standard/no-gain p-type detectors [18], the annealing decreases somewhat ($\lesssim 20\%$) the collected charge of the Ga-LGADs for ^{90}Sr electrons (see Fig. 10a).

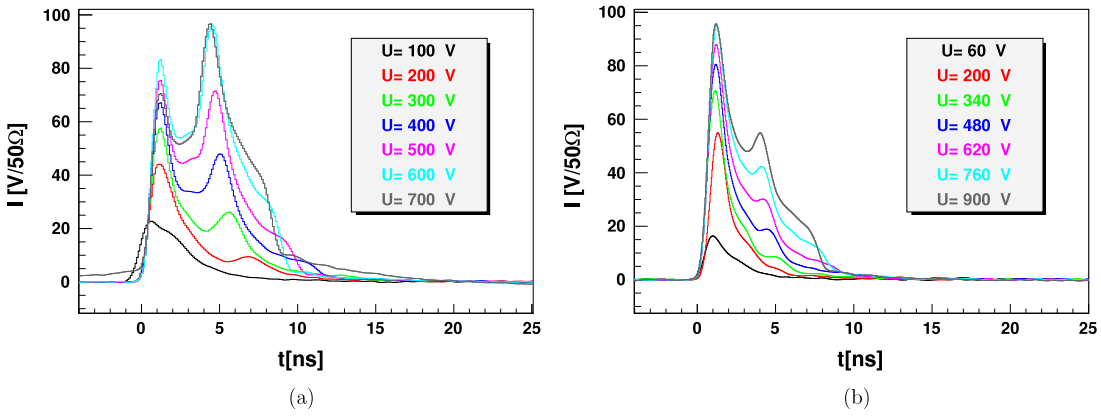

Fig. 8. (a) α TCT for Dose2 device irradiated to $1 \cdot 10^{15}$ cm^{-2} and (b) for Dose4 device irradiated to $2 \cdot 10^{15}$ cm^{-2}.

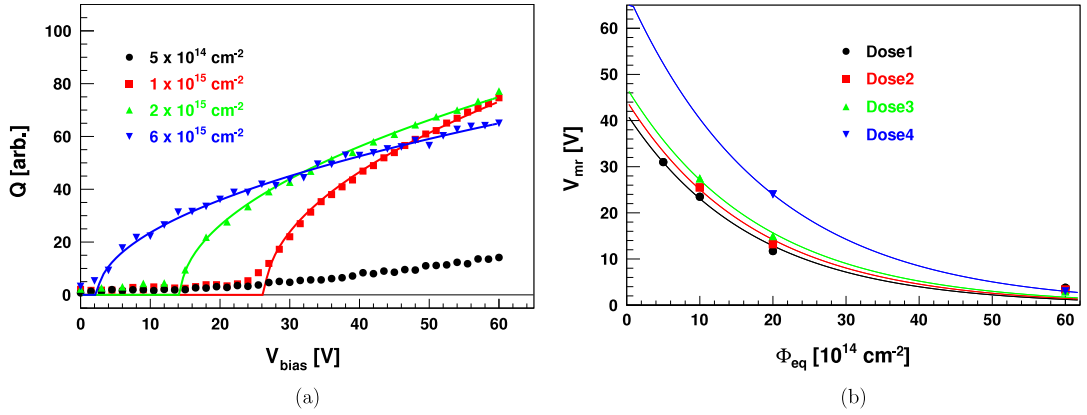

Fig. 9. (a) Dependence of induced charge on bias voltage for Dose2 devices at different fluences. The fit of $\sqrt{V_{bias} - V_{mr}}$ to the data is also shown. (b) Dependence of V_{mr} on equivalent fluence for different devices ($T = -10$ °C).

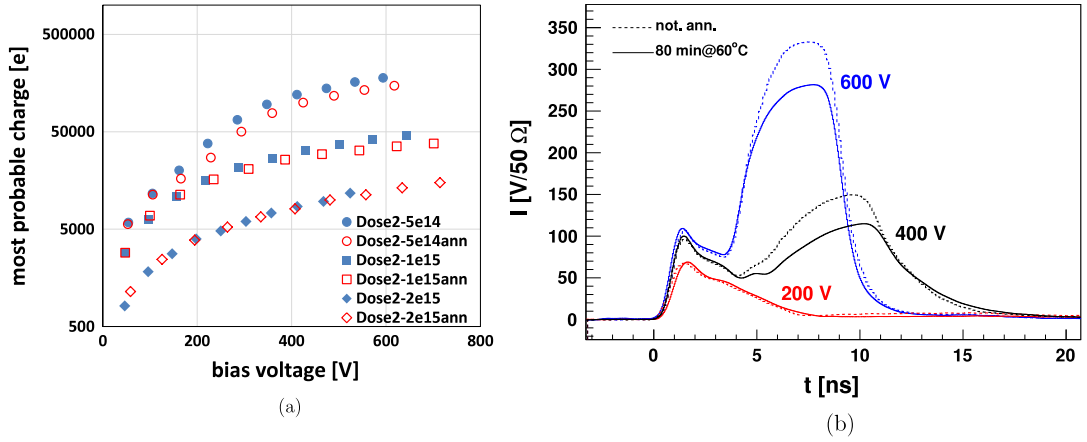

Fig. 10. (a) Dependence of most probable charge for ^{90}Sr electrons on voltage for Dose2 devices irradiated to different fluences before and after 80 min at 60° annealing ($T = -15$ °C). (b) Induced currents for α particles injected in the back of Dose2 detector irradiated to $5 \cdot 10^{14}$ cm^{-2} before and after annealing at $T = -10$ °C. The plots were not scaled-absolute measurements.

The difference in performance is related to the gallium doped multiplication layer rather than the boron doped bulk. This can be concluded from the α-TCT signals. The induced current pulses for the Dose2 device irradiated to $5 \cdot 10^{14}$ cm^{-2} are shown in Fig. 10b. Identical pulse shapes before the onset of multiplication indicate that the field in the bulk remains almost unchanged during short term annealing. The amplitude of the multiplied signal on the other hand decreases with annealing. The difference in gain cannot be explained by annealing of deep (radiation induced) acceptors as their concentration was too small at the investigated fluences. Therefore, the difference in gain must be gallium related. Hence, the removal rate c depends on annealing history and is slightly larger after short-term annealing than immediately after

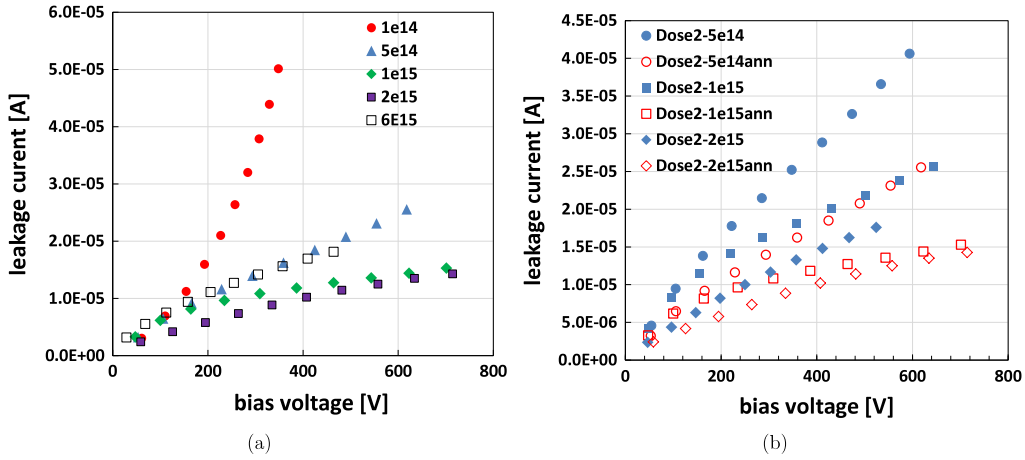

Fig. 11. (a) Leakage current vs voltage for annealed Dose2 devices irradiated to different fluences measured at $T = -15$ °C. (b) Effect of annealing on leakage current for Dose2 devices. The fluences given in the legend are in [cm^{-2}].

irradiation. Clearly more comprehensive annealing studies are required to establish the gain evolution in Ga-LGADs.

7. Leakage current

The leakage current in LGAD devices $I_{leak} = M \cdot I_{gen}$ [10] depends on the generation current I_{gen} as well as on the current gain M. Measured $I-V$ plots for Dose2 devices are shown in Fig. 11a. The leakage current decreases up to the fluence of $2 \cdot 10^{15}$ cm^{-2}. The decrease of gain with fluence dominates over the increase of generation current. The current starts to increase again for the highest fluence ($6 \cdot 10^{15}$ cm^{-2}), indicating that gain decrease does not compensate generation current increase anymore. The calculated generation current, $I_{\text{gen}} = \alpha \cdot S \cdot d \cdot \Phi_{\text{eq}}$ for the device with active area $S = 10.25$ mm^2 and thickness $d = 285$ μm, is ~ 8 μA after $\Phi_{\text{eq}} = 2 \cdot 10^{15}$ cm^{-2} ($\alpha(-15$ °C, 80 min at 60 °C) $= 1.2 \cdot 10^{-18}$ A/cm [19]). This value is around a factor of two lower than current measured at 600 V and is in agreement with an estimated gain of around 2 (see Section 3). Moreover, the leakage current for the highest irradiated sample at maximum voltage agrees very well with the calculated generation current implying no multiplication.

The decrease of leakage current with annealing is affected by both, gain and generation current decrease (see Fig. 11b), hence it is relatively larger than for standard p-type detectors.

8. Conclusions

First LGADs of standard thickness (285 μm) were produced with gallium replacing boron as shallow dopant in the multiplication layer. Due to unreliable process simulations, the concentration of gallium in the multiplication layer was too high causing an early break down of devices before irradiations. After irradiations, the decrease of gain and appearance of deep traps led to electric field profiles similar to those of forward bias detectors. Only after the gain decreased sufficiently, the devices performed similarly to standard boron doped LGAD devices. The removal rate of gallium was found to be $c \approx 5 \cdot 10^{-16}$ cm^2, around two times smaller than for so far studied boron LGAD detectors. This feature could lead to significantly improved performance of thin Ga-LGADs at HL-LHC. Higher initial dopant concentration and smaller removal rate led to sizable gains also at fluences $> 10^{15}$ cm^{-2}. Short term annealing decreases effective acceptor concentration in the multiplication layer, hence causing smaller gain.

Acknowledgments

Part of this work has been financed by the Spanish Ministry of Economy and Competitiveness through the Particle Physics National Program (FPA2015-69260-C3-3-R and FPA2014-55295-C3-2-R) and carried out under the Spanish ICTS Network MICRONANOFABS partially supported by MINECO. The support came also from the European Union's Horizon 2020 Research and Innovation funding program, under Grant Agreement no. 654168 (AIDA-2020).

References

[1] G. Pellegrini, et al., Technology developments and first measurements of Low Gain Avalanche Detectors, LGAD for high energy physics applications, Nucl. Instrum. Methods A 765 (2014) 12.
[2] G. Kramberger, et al., Radiation hardness of thin low gain avalanche detectors, Nucl. Instrum. Methods A 891 (2018) 68.
[3] G. Paternoster, Developments and first measurements of ultra-fast silicon detectors produced at FBK, J. Instrum. 12 (2017) C02077.
[4] N. Cartiglia, et al., Design optimization of ultra-fast silicon detectors, Nucl. Instrum. Methods A 796 (2015) 141.
[5] H. Sadrozinski, et al., Ultra-Fast Silicon Detectors, UFSD, Nucl. Instrum. Methods A 831 (2016) 18.
[6] N. Cartiglia, et al., Beam test results of a 16 ps timing system based on ultra-fast silicon detectors, Nucl. Instrum. Methods A 850 (2017) 83.
[7] Z. Galloway, et al., Properties of HPK UFSD after neutron irradiation up to 6e15 n/cm2, (2017). arXiv:1707.04961v3.
[8] CMS Collaboration, CMS phase II upgrade scope document, 2015. CERN-LHCC-2015-19.
[9] ATLAS Collaboration, ATLAS phase-II upgrade scoping document, 2015. CERN-LHCC-2015-020.
[10] G. Kramberger, et al., Radiation effects in low gain avalanche detectors after hadron irradiations, J. Instrum. 10 (2015) P07006.
[11] A. Khana, et al., Strategies for improving radiation tolerance of Si space solar cells, Sol. Energy Mater. Sol. Cells 75 (2003) 271.
[12] L. Snoj, G. Žerovnik, A. Trkov, Computational analysis of irradiation facilities at the JSI TRIGA reactor, Appl. Radiat. Isot. 70 (2012) 483.
[13] V. Eremin, N. Strokan, E. Verbitskaya, et al., Development of transient current and charge techniques for the measurement of effective net concentration of ionized charges (N-eff) in the space charge region of p–n junction detectors, Nucl. Instrum. Methods A 372 (1996) 388.
[14] G. Kramberger, V. Cindro, I. Mandić, et al., Effective trapping time of electrons and holes in different silicon materials irradiated with neutrons, protons and pions, Nucl. Instrum. Methods A 481 (2002) 297.
[15] G. Kramberger, V. Cindro, I. Mandić, et al., Charge collection properties of heavily irradiated epitaxial silicon detectors, Nucl. Instrum. Methods A 554 (2005) 212.
[16] V. Eremin, et al., The operation and performance of Current Injected Detector, CID, Nucl. Instrum. Methods A 581 (2007) 356.
[17] V. Eremin, et al., Current injected detectors at super-LHC program, Nucl. Instrum. Methods A 583 (2007) 91.
[18] K. Hara, et al., Charge collection and field profile studies of heavily irradiated strip sensors for the ATLAS inner tracker upgrade, Nucl. Instrum. Methods A 831 (2016) 181.
[19] M. Moll, et al., Leakage current of hadron irradiated silicon detectors - material dependence, Nucl. Instrum. Methods A 426 (1999) 87.